RSC Advances

ROYAL SOCIETY OF CHEMISTRY

www.rsc.org/advances

Title: Ultrathin tungsten oxide nanowires: oleylamine assisted nonhydrolytic growth, oxygen vacancy and high photocatalytic properties

Authors: Fenglin Liu, Xianjie Chen, Qinghua Xia, Lihong Tian and Xiaobo Chen

Ultrathin tungsten oxide nanowires with the diameter of around 1.1 nm have been fabricated through a simple oleylamine (OA) assisted nonhydrolytic process. In the process, the amount of OA played an important role on controllable formation of tungsten oxide ultrathin nanowires.

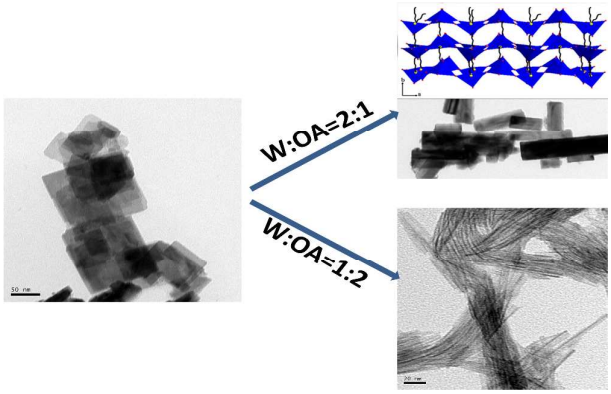

Journal Name

ARTICLE

Ultrathin tungsten oxide nanowires: oleylamine assisted nonhydrolytic growth, oxygen vacancy and high photocatalytic properties

Received 00th January 20xx,
Accepted 00th January 20xx

DOI: 10.1039/x0xx00000x

www.rsc.org/

Fenglin Liu[a], Xianjie Chen[a], Qinghua Xia[a], Lihong Tian[a,b]*and Xiaobo Chen[b]*

Ultrathin tungsten oxide nanowires with the diameter of around 1.1 nm have been fabricated through a simple oleylamine (OA) assisted nonhydrolytic process. In the process, the amount of OA, reaction temperature and time impacted on controlling the formation of tungsten oxide ultrathin nanowires. At high W/OA molar ratios (> 1 : 1), oriented attachment of OA molecule resulted in the preferential growth of nanowires along the [001] direction. At low W/OA molar ratios, small nanoparticles self-assembled into ultrathin nanowires. The ultrathin tungsten oxide nanowires exhibited a high photocatalytic activity on the degradation of Rhodamine B under visible light, likely due to their enhanced visible-light absorption and the presence of oxygen vacancy.

1. Introduction

The photocatalytic oxidation technology utilizing solar energy has attracted increasing interests in decomposing various environmental contaminants [1]. Compared with the TiO_2, the most popular photocatalyst, tungsten oxide can extend the absorbance to the blue region of the solar spectrum, as it has a band gap energy of around 2.4-2.8 eV [2] and its deep valence band edge (3.1 eV) is much more positive than the H_2O/O_2 oxidation potential and suitable for photo-oxidising organic pollutants under visible light [3]. Nevertheless, conduction band level of WO_3 (0.5 eV vs NHE) is more positive than the potential for the single-electron reduction of oxygen, leading to the low light energy conversion efficiency because of high recombination of excited electrons and holes [4]. Up to now, several approaches have been taken to solve the problem: such as platinum loading to induce a multielectron O_2 reduction [5]; carbon materials (carbon nanotube and graphene) composites to improve the photocatalytic activity by forming W-C bond to benefit the electron transfer [6]; advanced nanoarchitecture tuning to increase surface area and pores, etc [7].

One-dimension (1D) nanomaterials, such as nanowires, nanobelts and nanorods are one of the hot research topics in modern materials science, chemistry, and physics, due to their high surface area, reduced grain boundaries, direct charge transfer pathways, and strong quantum size effects [8]. Especially, the short charge diffusion length and more reactive sites in ultrathin nanowires bring in fantastic properties in photocatalysis [9]. Non-hydrolytic approaches have been successfully taken to control the morphology, dimensions and particle size of nanomaterials. Recently, some achievements on ultrathin nonstiochiometric tungsten oxide was also obtained through it, particularly, $W_{18}O_{49}$ nanowires. For instance, Brian et. al synthesized the nonstiochiometric tungsten oxide nanowires with diameter of 1-4 nm by controlling the ratios of W $(CO)_6$, octadecanol and octadecene [10]. Ye et al. obtained $W_{18}O_{49}$ nanowires with diameter of 0.9 nm with WCl_6 precursor in ethanol [11]. Niederberger and co-workers achieved the preferential growth of $W_{18}O_{49}$ along [010] direction and obtained nanowires with a diameter of 1.3 nm with deferoxamine coordinating with tungsten atoms [12]. However, controlled synthesis of ultrathin tungsten oxide nanowires with the diameter closing to one cell unit size (< 2nm) is of great interest for enhancing photocatalytic activity. Moreover, it is also vital to clarify their growth mechanism for extending their applications.

In this work, we presented an oleylamine (OA)-assisted synthesis of ultrathin tungsten oxide nanowires in benzyl alcohol (BA) solution. Three critical factors, the amount of oleylamine, reaction temperature and time, were investigated

[a] L. Liu, X. Chen, Prof. Dr. Q. Xia, Dr. L. Tian
Hubei Collaborative Innovation Center for Advanced Organochemical Materials, Ministry-of-Education Key Laboratory for the Synthesis and Applications of Organic Functional Molecules, Hubei University, Wuhan 430062,China
E-mail: tian7978@hubu.edu.cn (L. Tian)
[b] Dr. L. Tian, Prof. Dr. X. Chen
Department of Chemistry, University of Missouri – Kansas City, Kansas City, Missouri 64110, USA
E-mail: chenxiaobo@umkc.edu (X. Chen)
† Footnotes relating to the title and/or authors should appear here.
Electronic Supplementary Information (ESI) available: [details of any supplementary information available should be included here]. See DOI: 10.1039/x0xx00000x

to figure out the growth mechanism of ultrathin nanowires in detail. The diameter of nanowires could be reduced to around 1 nm and the length can reach several micrometers. Moreover, the photocatalytic performance of ultrathin nanowires was also studied in visible light region.

2. Results and discussion

2. 1 XRD patterns and Raman spectra

The simple one-spot synthesis with tungsten chloride in benzyl alcohol resulted in the formation of a yellow-green powder (reference sample), which was characterized by XRD and shown in Fig.1a. The sharp and intensive peaks indicated a highly crystalline nanostructure. The obvious diffractive peaks with 2θ at 23.1°, 23.7°, 24.2°, 34.1° corresponded to the (002), (020), (200), and (202) crystal planes of monoclinic phase of WO_3 with lattice parameters of a = 7.297, b = 7.539, and c = 7.688 Å (JCPDS no. 43-1035) [13], respectively, which is different from Niederberger's report [14]. Interestingly, with the addition of oleylamine and when the molar ratio of WCl_6 to OA was 0.5, only the diffractive peaks of (002) plane was observed and the other reflections were much weak, thus manifesting tungsten oxide nanowires selectively grew along the [002] direction [15]. Here, it was difficult to assign the nanowire to special crystal structure from XRD pattern because amount of stoichiometric or nonstoichiometric tungsten oxide had rather similar structure [16].

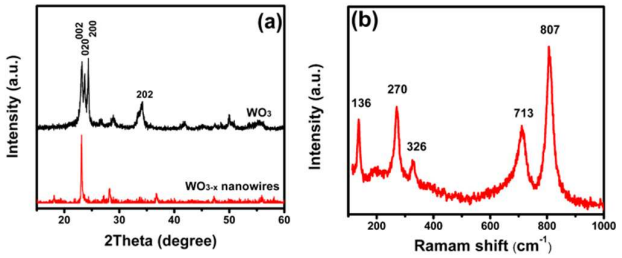

Fig. 1. (a) XRD patterns of WO_3 (reference sample) and WO_{3-x} (1-2) nanowire, and (b) Raman spectrum of the WO_{3-x} (1-2) nanowire.

The Raman spectrum of the tungsten oxide nanowires is shown in Fig.1b. The strong and well-defined bands at 807, 713, 326, 270 cm^{-1} could be assigned to monoclinic tungsten oxide, which could support the XRD results. The bands at 270 cm^{-1} correspond to O-W-O bending modes, and the bands at 713 and 807 cm^{-1} are ascribed to the stretching modes of the W-O-W [17]. The relatively strong peak observed at low frequency (136 cm^{-1}) and the weak band at 326cm^{-1} were attributed to the O-O deformation and W-O deformation modes, respectively [18], indicating the anisotropic atoms aligning on the surface of nanowires.

2.2 XPS and FT-IR spectra

XPS spectra were conducted to detect the surface composite and valence of elements in tungsten oxide nanowires. It can be seen from Fig. 2a that W and O were the main constituent elements and carbon probably came from the impurity of XPS detect and residual organic molecule. The W4f XPS spectra in Fig. 2b presented two strong peaks at the binding energy of 35.3 eV and 37.3 eV matched well with reported values of the W^{6+} oxidation state for WO_3 nanosheets [19], whereas a distinct difference shown in the fitted curves of WO_{3-x} nanowires that two peaks corresponding to W^{6+} shifted to much higher binding energy (35.8 eV and 37.8 eV), indicating the presence of W-O-N bond [20]. The linkage of W atoms and oleylamine (W-O-N) likely induced the charge imbalance of W-O and resulted in the surface defect, even the color change (see following UV-vis DRS results). More importantly, two peaks occurred at relatively low binding energy (34.8 eV and 33.3 eV), revealing the existence of W^{5+} and W^{4+} in nanowires, accompanying with the appearance of oxygen vacancy [21]. Also, an obvious difference was shown in Fig. 2c: the O1s spectrum of WO_3 nanosheets demonstrated the obvious peaks ascribed to lattice oxygen (530.0 eV) and the hydroxyl groups (532.0 eV). Unlike WO_3 nanosheets, the band of lattice oxygen up-shifted to 530.7 eV and a new peak at 528.7eV was possibly attributed to the W-O-N bond. The shifts of both W4f and O1s in nanowires indicated that the chemical environment of W and O atoms in nanowires changed compared with that WO_3 nanosheets and likely resulted in the deformation of W-O and O-O bond, coincident with the Raman investigation.

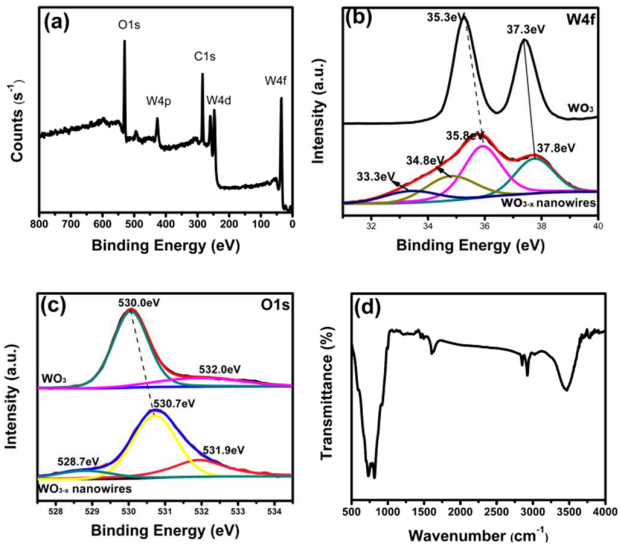

Fig. 2 (a) the whole spectroscopy of WO_{3-x} (1-2) nanowires, (b)W4f and (c) O1s XPS spectra of WO_3 (reference sample) and WO_{3-x} (1-2) nanowires, (d) FT-IR spectrum of WO_{3-x} (1-2) nanowires.

The FT-IR spectrum of tungsten oxide nanowires was shown in Fig. 2d. The strong bands in the region of 1000-500 cm^{-1} were assigned to the characteristic stretching vibrations of W-O (950 cm^{-1}) units and the bridging oxygen atoms O-W-O (600-780 cm^{-1}) [22]. The peaks at 1626 and 3400 cm^{-1} came from the physically adsorbed water and the hydroxyl groups. Two vibrations at 2921 cm^{-1} and 2844 cm^{-1} were attributed to the $-CH_3$ and $-CH_2$ stretching vibrations, indicating the presence

of residual oleylamine molecule on the surface of tungsten oxide.

2. 2 Morphology and structure

For further investigate the structure of WO_{3-x} nanowires, TEM and HRTEM micrographs were performed and shown in Fig. 3. The reference sample WO_3 synthesized by benzyl alcohol route were nanosheets with size of 100-200nm (Fig. 3a). Nevertheless, WO_{3-x} nanowires were achieved with the control of oleylamine (Fig. 3b). The diameter of nanowires was uniform and around 1.9 nm, but the length, from 200 nm to several micrometers, could not be estimated accurately on account of the twisted bundles in Fig. 3b. Also, the clear lattice fringes in Fig. 3c (HRTEM) verified the highly crystalline tungsten oxide nanowires. An interplanar d-spacing of 0.383 nm should be ascribed to (002) crystal plane of monoclinic WO_3, revealing nanowires grew along the c axis (Fig. 3d), which was in good agreement with the XRD results. The selected area electron diffraction pattern in the inset only showed one intense diffraction ring, corresponding to the 002 reflection of the WO_{3-x} nanowires. All other diffuse and broad diffraction rings were attributed to the much weak reflections. The electron-induced X-ray fluorescence (EDX) analysis was employed to determine the composition of the tungsten oxide nanowires (see supporting information Fig. S1). There were oxygen, tungsten and carbon elements existed in the nanowires. The signal of carbon probably came from the residual organic compound.

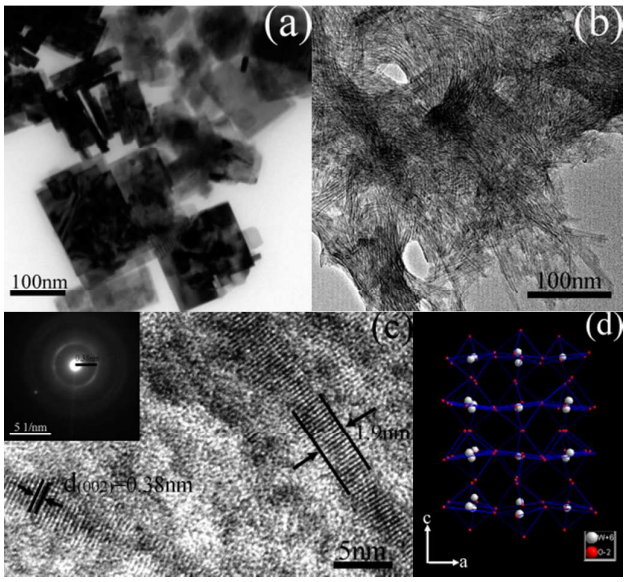

Fig. 2 (a) TEM image of WO_3 (reference sample), (b) TEM image of WO_{3-x} (1-2) nanowires, (c) HRTEM micrograph, and SAED pattern (the inset) of WO_{3-x} (1-2) nanowires, and (d) schematic representation of monoclinic WO_3 along c axis.

2.4 TG-DTA analysis

The thermal behaviour of the samples was studied by TG-DTA analyses in an air atmosphere with a heating rate of 10 °C/min and displayed in Fig.4. The weight loss up to 350 °C might be assigned to desorption of surface-adsorbed water, structural water elimination and physically adsorbed organic molecule for both samples [23]. It is noteworthy that WO_3 (1-2) nanowires showed a dramatic weight loss about 17% compared to that of WO_3 nanosheets between 350-500 °C, attributed to the loss of surface capped OA molecule.

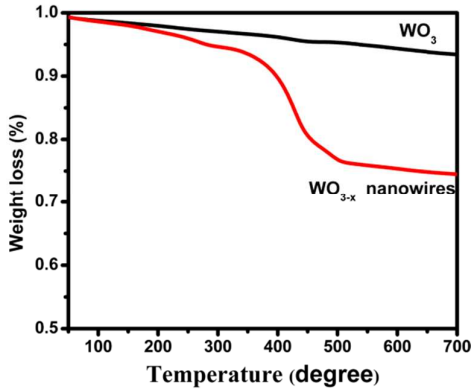

Fig. 4 TG-DTA curves of the WO_3 (reference sample)and WO_{3-x} (1-2) nanowires.

2. 5 Growth of WO_{3-x} nanowires

It is known that the synthesis of nanostructure usually encounters with many sensitive reaction parameters. In order to clarify the growth mechanism of WO_{3-x} nanowires, three main factors, the concentration of oleyamine, reaction temperature and time, are investigated in detail here.

Using benzyl alcohol (BA) as the solvent and WCl_6 as the precursor, the controllable synthesis of tungsten oxide nanowires could be achieved by straightforward solvothermal method with the aid of OA. Fig. 5 clearly demonstrates the morphology transfer of tungsten oxide from nanosheets to nanowires with increasing the amount of oleylamine. WO_3 nanosheets assembled by small grains were obtained via benzyl alcohol route under the condition of 180 ^{o}C and 24 h (Fig. 5a). However, with low concentrations of OA (i.e. molar ratio of W: OA = 2 : 1), nanosticks with widths of 15-30 nm and lengths of around 63-200 nm were formed, and moreover, the surface of nanosticks were crude (Fig. 5b). At higher OA concentrations, such as moral ratio of W: OA = 1 : 1, it seemed that nanosticks were stripped into the nanowires gradually and some short wires were visible in Fig. 5c. When the moral ratio reached 1 : 1.5, uniform nanowires were formed with the diameter of about 1.1 nm and length of 100 nm (Fig. 5d), which was roughly same to the length of nanosticks in Fig. 5b. Much longer nanowires (> 300 nm) grew at the moral ratio of W : OA = 1 : 2, but the diameter did not change (Fig. 5e). Nanowires began to be cut into short segments with the excess OA content (W : OA = 1: 2.5) (Fig. 5f). Accordingly, oleylamine contributed to the formation of ultrathin tungsten oxide nanowires, and their diameter and length can be tailored by simply adjusting the moral ratio of WCl_6 to OA.

In addition, an interesting shift of XRD diffractive peaks of tungsten oxides took place in the presence of oleyamine (see the supporting information Fig. S2). At the low OA concentration (molar ratio of W: OA = 2 : 1), the main diffractive peaks of (002), (020) and (200) shifted 4° to low diffraction angle, indicating the OA molecule entered into the crystal lattice and likely resulting in the lattice expansion of tungsten oxide. With the increasing of OA concentration, the peaks ascribed to (020) and (200) planes wore off and the (002) peak intensified, ultimately monoclinic WO_{3-x} nanowires grew.

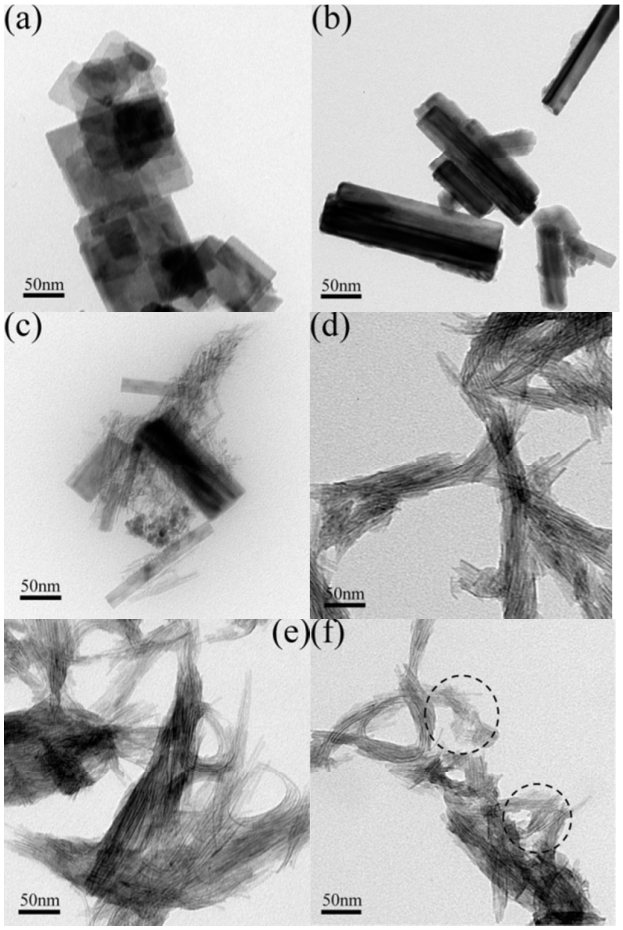

Fig. 5 TEM images of all tungsten oxide synthesized with different moral ratio of WCl_6 to OA at 180°C, 24h. (a) without OA, (b) W : OA=2 : 1, (c) W : OA=1 : 1, (d) W : OA=1 : 1.5, (e) W : OA=1:2, and (f) W : OA=1 : 2.5.

Also, the effects of reaction time and temperature on the formation of nanowires were studied at the condition of W: OA = 1 : 2 (molar ratio) to figure out the optimal growing condition of tungsten oxide nanowires. We found that reaction time impacted the length of nanowires. As shown in Fig.6, after the solvothermal reaction for 6 h at 180℃, only short WO_3 nanorods with an average length of 20-50 nm accompanying nanoparticles formed (Fig. 6a); the 18h reaction led to slightly longer WO_{3-x} nanowires and small amount of them attained 160 nm (Fig.6b); growth for 24h produced nanowires with length > 300 nm (Fig. 5e). However, the longer reaction time (i.e. 30 h) resulted in the nanowires tangled with each other (Fig. 6c). In addition, relatively low temperature brought about tungsten oxide bundles (Fig.6d), which was likely related to high boil point of OA and not fully extended C-C chain in low temperature [24].

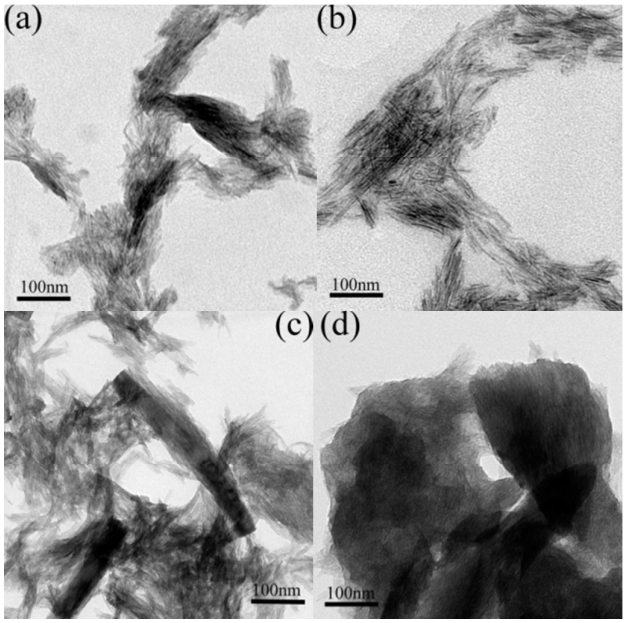

Fig.6 TEM images of WO_3 (1-2) synthesized with different reaction time and temperature at 180°C. (a) 6h, (b) 18h, (c) 30h, (d) at 150°C, 24h.

Benzyl alcohol solvent has been proven to provide a decent environment to synthesize and tailor the shape and structure of metal oxide nano-architectures with the help of organic capping regents [25]. In our experiments, byproducts, benzaldehyde (m/z=106), benzyl chloride (m/z=126) and benzyl ether (m/z=198), were detected (GC-MS results). Accordingly, the growth of tungsten oxide underwent the process that WCl_6 reacted with benzyl alcohol firstly to produce the tungsten alkoxide, then the condensation of tungsten alkoxide to form W-O-W unit, thus WO_3 nanosheets emerged. This process is proposed as follows:

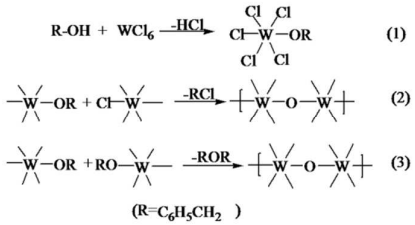

It was similar to the other reported synthesis of metal oxide by nonhydrolytic method [26]. However, in the presence of oleyamine, the preferential growth direction of tungsten oxide surprisingly changed. So it is interesting to see through the

growth pathway of nanowires clearly. Based on the above results and the crystal structure of monoclinic WO_3, we inferred that oriented attachment of OA molecule on the (020) plane of monoclinic WO_3 was responsible to the tungsten oxide nanowires, as a large number of tungsten atom centrally located in (020) plane and oxygen atom mainly distributed in the cross section of (002) and (200) planes (see the supporting information Fig. S3). As shown in Scheme.1, at low OA concentration, OA molecule inserted into lamellar spacing and coordinated with the W atom in (020) plane, limiting the crystal growth along b axis at a certain extent, thus leading to the nanosticks (Fig. 5b). While increasing the amount of OA molecule could destroy the nanosticks because of the strong mutual repulsion between the long C-C chains of OA, and prevent the formation of W-O-W unit along a axis due to the coordination of W atoms and OA. Consequently, small nanocrystals produced and self-assembled into ultrathin nanowires along c axis. This could be confirmed by TEM image of nanowires in formamide, where only small uniform nanoparticles can be observed (see supporting information Fig. S4).

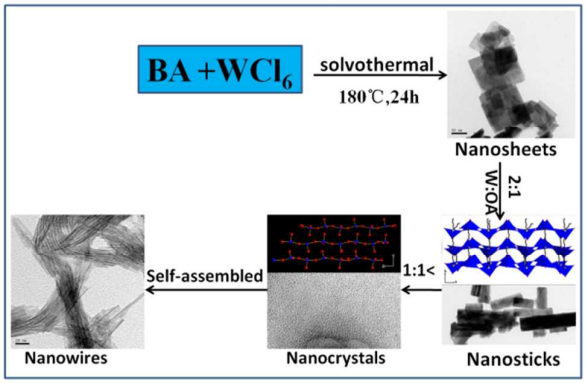

Scheme 1. The proposed growth process of WO_{3-x} nanowires

2.6 Photocatalytic activity of WO_{3-x} nanowires

The photocatalytic activity of WO_{3-x} nanowires is evaluated by the photodegradation of RhB dye under visible light irradiation. As seen from Fig. S5a (see supporting information), WO_3 nanosheets showed very poor visible-light photocatlytic activity. The obtained products in the presence of OA manifested only slightly enhanced activity until the molar ratio of W: OA attained the 1 : 1.5, that is, ultrathin nanowires presented the significantly increased photoactivity under visible light. Apparently, the ultrathin WO_3 (1-2) nanowires with diameter about 1.1 nm showed the highest photocatalytic activity of WO_{3-x} nanowires. In our experiment, BET surface area is not the main contribution to the high photocatalytic activity because nanowires showed a relatively low BET surface area compared with reference WO_3 nanosheets (see the supporting information Table S1), which likely related to the capped OA molecule on the surface WO_{3-x} nanowires. Thus, the high photocatalytic activity possibly ascribed to the enhanced absorption and oxygen vacancy. As shown in Fig. S5b (see supporting information), all samples obtained with the existence of OA had enhanced absorption in visible light region, matching with the color change from yellow-green to blue. Moreover, it is noted that all tungsten oxide nanowires (W : OA < 1 : 1.5) exhibited a tailed absorption, likely indicating the existence of oxygen vacancy on nanowires. They can likely promote the enhanced absorption and separation of electrons and holes and led to the enhanced photocatalytic activity [27].

3. Experimental section

3.1 Synthesis of ultrathin tungsten oxide nanowires

The tungsten oxide nanowires were synthesized by OA assisted solvothermal method. All chemicals were of analytical grade and used without further purification. Briefly, 0.8 g WCl_6 was quickly placed into mixed solution of 40 ml benzyl alcohol and a desired content of OA by vigorously stirring. The color of solution changed from yellow to dark blue. Subsequently, the solution was transferred into a Teflon-lined, stainless autoclave at 180 ℃ for 24 h. The powders were washed with acetone, absolute ethanol and deionized water several times, then dried at 70 ℃ for a day. The final product was collected and denoted as WO_{3-x} (a-b), wherein a-b is the molar ratio of WCl_6 to OA. The reference WO_3 sample was prepared under the same condition without oleyamine.

3. 2 Characterizations

The crystalline structure of as-prepared samples was determined by X-ray powder diffraction (XRD, Bruker D8 advance), with Cu Kα radiation (λ = 1.54 Å) at the scan rate of 5 ° min^{-1} with a step of 0.02 °. Morphologies of samples were studied by transmission electron microscopy (TEM, *FEI*, Tecnai G20) and a JEM-2100UHR high-resolution transmission electron microscope (HRTEM). X-ray photoelectron spectroscopy (XPS) measurements were carried out using a VG Multilab 2000 spectrometer with an Al Ka X-ray source (Thermo Electron Corporation), and all the spectra were calibrated to the C 1s peak at 284.6 eV. The UV–Vis diffuse reflection spectra were obtained for the dry-pressed disk samples on a UV–vis spectrophotometer (UV-2550) by $BaSO_4$ as the reflectance sample. Raman spectra were recorded on a laser micro-Raman spectrometer (Invia, Renishaw). Fourier transform infrared spectroscopy (FT-IR) spectra were obtained on a Nicolet IS10 spectroscope to investigate the surface organic species on all tungsten oxide. Simultaneous thermogravimetric and differential thermal analyses (TGA/DTA) of the samples were performed on a thermal analyzer (SDT Q600) in air with a heating rate of 10 ℃/ min^{-1} in air atmosphere. Gas chromatography–mass spectrometry (GC/MS, QP2010, Ultra) was used to analyzed the by-products in the nonhydrolytic synthesis. BET surface area of samples was performed on a surface area and porosity analyzer (GWGB SCI & TECH, BK112T). Prior to the BET analysis, the powder samples were degassed at 200 °C for 2 h to remove the adsorbed H_2O from the surface.

3. 3 Photocatalytic test

The photocatalytic performance of all samples was evaluated by degrading Rhodamine B (RhB) using a 300 W high-pressure xenon lamp (CEL-HXF300). In a typical experiment, 10 mg of photocatalysts were suspended in 50mL of 10 mg·L^{-1} RhB aqueous solution. Before light irradiation, the suspension was sonicated for 30 min and stirred for an hour in the dark to ensure the establishment of the adsorption / desorption equilibrium of RhB on the catalyst surface. Then, the solution was placed in a quartz reaction vessel and bubbled with air. At given time intervals, 5 mL solution was taken out and centrifuged. The concentration of RhB was monitored by colorimetry using a UV-Vis spectrophotometer (UV-2550).

4. Conclusions

In conclusion, we have successfully prepared ultrathin tungsten oxide nanowires with the aid of OA. The molar ratio of WCl_6 to OA played an important role on controlling the formation of tungsten oxide nanowires. At low OA concentration, OA selectively attached on the (020) plane of monoclinic WO_3, resulting in WO_3 nanosheets changed into nanosticks. However, when the molar ratio of W : OA < 1 : 1.5, small nanocrystals self-assembled into ultrathin nanowires. Reaction time only decided the length and temperature had a significant effect on the dispersion of nanowires, thus the optimal reaction condition is that molar ratio of W : OA = 1 : 2, 180℃ for 24h to obtain uniform tungsten oxide nanowires with the diameter of around 1.1 nm and length of several micrometers. In addition, ultrathin tungsten oxide nanowires exhibited larger absorption in visible light than WO_3 nanosheets and high photocatalytic performance on degradation of RhB under visible light.

Acknowledgements

L. Tian gratefully acknowledges the support from National Natural Science Foundation of China (No. 51302072), Natural Science Foundation of Hubei Provincial Department of Education (No. Q20131010), Natural Science Fund for Creative Research Groups of Hubei Province of China (No. 2014CFA015). X. Chen thanks the support from College of Arts and Sciences, University of Missouri - Kansas City and the University of Missouri Research Board.

Notes and references

1 a)M. R. Hoffmann, S. T. Martin, W. Choi, D. W. Bahnemannt, *Chem. Rev.*, 1995, **95**, 69; b)X. Chen, S. Shen, L. Guo, S. S. Mao, *Chem. Rev.*, 2010, **110**, 6503.
2 a) Z. Zhao, M. Miyauchi, *Angew.Chem.*, 2008, **120**, 7159; b) X. Chen, S. S. Mao, *Chem. Rev.*, 2007, **107**, 2891.
3 R. Abe, H. Takami, N. Murakami, B. Ohtani, *J. Am. Chem. Soc.*, 2008, **130**, 7780.
4 D. E. Scaife, *Solar Energy.*, 1980, **25**, 41.
5 a) J. W. Liu, J. H. Zhu, C. L. Zhang, H.W. Liang, S. H. Yu, *J. Am. Chem. Soc.*, 2010, **132**, 8945; b) J. Kim, C. W. Lee, W. Choi, *Environ. Sci. Technol.*, 2010, **44**, 6849.
6 a)L. Tian, L. Ye, J. Liu, L. Zan, *Catal. Commun.*, 2012, **17**, 99; b) O. Akhavan, M. Choobtashani , E. Ghaderi, *J. Phys. Chem. C.*, 2012, **116**, 9653.
7 a) H. Zheng , J. Z. Ou , M. S. Strano , R. B. Kaner , A. Mitchell , K. Kalantar-zadeh, *Adv. Funct. Mater.*, 2011, **21**, 2175; b) B. Moshofsky, T. Mokari, Chem. Mater. 2013, **25**, 1384.
8 a) S. Hu, X. Wang, *Chem. Soc. Rev.*, 2013, **42** , 5577-5594; b) T. Ruecks, K. Kim, E. Joselevich, G. Y. Tseng, C. Cheung, C. M. Lieber, *Science*., 2000, **289**, 84.
9 M. H. Huang, S. Mao, H. Feick, H. Yan, Y. Wu, H. Kind, E. Weber, R. Russo, P. Yang, *Science.*, 2001, **292**, 1897.
10 J. Liu, O. Margeat, W. Dachraoui, X. J. Liu, M. Fahlman, J. Ackermann1, *Adv. Funct. Mater.*, 2014, **24**, 6029.
11 G. Xi, S. Ouyang, P. Li, J. Ye, Q. Ma, N. Su, H. Bai, C. Wang, *Angew. Chem. Int. Ed.*, 2012, **51**, 2395 –2399.
12 J. Polleux, N. Pinna, M. Antonietti, M. Niederberger, *J. Am. Chem. Soc.*, 2005, **127**, 15595-15601.
13 a) T. Nutz, M. Haase, *J. Phys. Chem. B.*, 2000, **104**, 8430 ; b) J. W. Seo, Y.W. Jun, S. J. Ko, J. Cheon, *J. Phys. Chem. B.*, 2005, **109**, 5389.
14 J. Polleux, A. Gurlo, N. Barsan, U. Weimar, M. Antonietti, M. Niederberger, *Angewandte. Chemie*, 2006, **118**, 267-271.
15 Z. Chen, Q. Wang, H. Wang, L. Zhang, G. Song, L. Song, J. Hu, H. Wang, J. Liu, M. Zhu, D. Zhao, *Adv. Mater.*, 2013, **25**, 2095-2100 .
16 G. L. Frey, A. Rothschild, J. Sloan, R. Rosentsveig, R. Popovitz-Biro, R. Tenne, *J. Solid State Chem.*,2001, **162**, 300.
17 F. D. Hardcastle and I. E. Wachs, J. Raman. Spectrosc. 1995, **26**, 397.
18 J. Y. Luo, S. Z. Deng, Y. T. Tao, F. L. Zhao, L. F. Zhu, L. Gong, J. Chen, N. S. Xu, *J. Phys. Chem. C.*, 2009, **113**, 15877 .
19 M. Sun, N. Xu, Y. W. Cao, J. N. Yao, E. G. Wang, *J. Mater. Res.*, 2000, **15**, 927.
20 P. J. Kulesza, L. R. Faulkner, *J. Electroanal. Chem.*, 1988, **248**, 305-320.
21 a) C. S. Blackman, I. P. Parkin, *Chem. Mater.* 2005, **17**, 1583-1590; b) D. Gogova, L. K. Thomas, B. Camin, *Thin Solid Films* 2009, **517**, 3326-3331.
22 A. Tocchetto, A.Glisenti, *Langmuir,* 2000, **16**, 6173-6182.
23 C. Guo, S. Yin, M. Yan, M. Kobayashi, M. Kakihana, T. Sato, *Inorg. Chem.*, 2012, **51**, 4763-4771.
24 T. He, Y. Ma, Y. Cao, X. Hu, H. Liu, G. Zhang, W.Yang, J. Yao, *J. Phys. Chem. B.*, 2002, **106**, 12670.
25 L. Cademartiri, G. A. Ozin, *Adv. Mater.*, 2009, **21**, 1013.
26 M. Feng, A. Pan, H. Zhang, Z. Li, F. Liu, H. Liu, D. Shi, B. Zou, H. Gao, *Appl. Phys. Lett.*, 2005, **86**, 141901.
27 a) I. Nakamura, N. Negishi, S. Kutsuna, T. Ihara, S. Sugihara, K. Takeuchi, *J. Mol. Catal. A: Chem.* 2000, **161**, 205-212; b)X. Pan, M. Yang, X. Fu, N. Zhang, Y. Xu, *Nanoscale*, 2013, **5**, 3601-3614; c) L. Ye, L. Zan, L. Tian, T. Peng, J. Zhang, *Chem. Commun.*, 2011, **47**, 6951-6953.

